POLYOXOMETALATES

Open Access
RESEARCH ARTICLE

Polyoxometalate-based Cu(II) complexes as the photocatalyst for oxidation of toluene and photodegradation of metronidazole

Fei Wang[1], Chaojun Jing[1] ✉, Jiejie Ping[1], Danyang He[1], Wenhui Shang[1], Muling Zeng[2] ✉, Nan Wang[1] ✉, and Zhiyu Jia[1] ✉

[1] *Key Laboratory of Cluster Science, Ministry of Education of China, Beijing Key Laboratory of Photoelectronic/Electrophotonic Conversion Materials, School of Chemistry and Chemical Engineering, Beijing Institute of Technology, Beijing 100081, China*
[2] *Institute of Materials Science of Barcelona, Campus de la UAB, 08193 Bellaterra, Spain*

Cite This: *Polyoxometalates*, **2024**, *3*, 9140067

Read Online

ABSTRACT: Polyoxometalates (POMs), renowned for their robust multielectron transfer capabilities, are utilized as photocatalysts. A Cu&POM based complex comprising $H_3PMo_{12}O_{40}$ (PMo_{12}) and 1,10-phenanthroline has been structured into a supramolecular framework through hydrogen bonding and π–π interactions. This complex demonstrates exceptional photocatalytic efficacy in the oxidation of toluene and the photodegradation of metronidazole. The oxidation of toluene with Cu-PMo_{12} achieved a yield and selectivity of 100% under low energy conditions, producing unprecedented results and demonstrating outstanding stability in cycling tests. Photodegradation of metronidazole using Cu-PMo_{12} achieved a degradation rate of 0.178. This work could facilitate the design and synthesis of novel Cu&POM based complexes with superior photocatalytic activities.

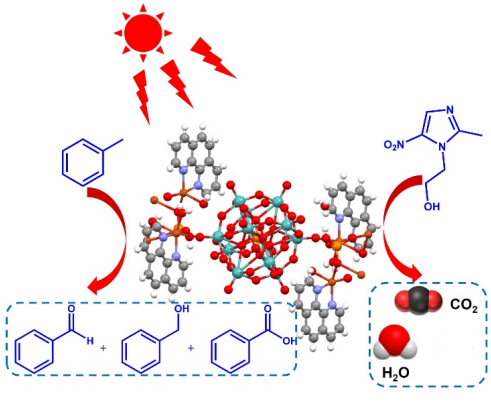

KEYWORDS: polyoxometalates, Cu-based complex, photocatalysis, photodegradation, mechanism

1 Introduction

Wastewater containing both inorganic and organic contaminants poses significant environmental challenges, jeopardizing human health due to their toxicity, persistence, and bioaccumulation [1, 2]. Consequently, the removal of pollutants has become a critical research focus in the field of water treatment. Among various methods, such as physical, chemical, and biological processes, photocatalytic treatment stands out as one of the most effective and promising techniques for eliminating organic contaminants [3, 4]. Notably, toluene, a common organic solvent, and metronidazole (MTZ), an antibiotic, have become prominent pollutants in recent decades [5, 6].

Achieving the oxidation of toluene and photodegradation of metronidazole presents an effective and appropriate method for water treatment. The photocatalytic oxidation of toluene yields commercially valuable products such as benzyl alcohol, benzaldehyde, and benzoic acid, which are versatile intermediates in the manufacture of preservatives, perfumes, dyes, pharmaceuticals, solvents, plasticizers, and flame retardants [7, 8]. Among these products, benzaldehyde is particularly desirable because it can be easily converted into the corresponding carboxylic acid [9]. Furthermore, the presence of MTZ in ground and surface water is increasing, posing potential risks to human health and the ecological environment [10]. Over the past decades, a highly efficient and low-cost photocatalytic method has been utilized for water treatment [11, 12]. Cu, an inexpensive, abundant, and redox-active transition metal, has been explored in various Cu-based complexes for applications such as water oxidation [13] and CO_2 reduction [14]. The interest in developing the properties of Cu-complexes has been growing [15]. Polyoxometalates (POMs), with their tailored structural and semiconducting properties, have been extensively applied as photocatalysts due to their unique ability to continuously accept electrons or protons while maintaining structural integrity and their powerful multielectron transfer capability [16–23]. POMs are instrumental in various applications including CO_2 photoreduction [24] and photocatalytic water splitting [25, 26]. Notably, POMs exhibit a high-energy excited state conducive to C–H activation [27, 28]. The helical microporous nanorods (HMNRs), assembled from POM clusters $[\alpha\text{-}P_4W_{18}O_{62}]^{6-}$ and cationic surfactants, have been utilized as photocatalysts for the oxidation of toluene [29]. Furthermore, numerous POM based complexes have demonstrated potential for use in photocatalytic degradation [30, 31]. For instance, two $\{As_3W_3\}$ polyoxometalates decorated with metal-phen complexes have shown outstanding

Received: January 16, 2024; **Revised:** May 4, 2024
Accepted: May 13, 2024

✉Address correspondence to Chaojun Jing, jingcj@bit.edu.cn; Muling Zeng, mulingzeng@163.com; Nan Wang, nanwang@bit.edu.cn; Zhiyu Jia, jzy@bit.edu.cn

photocatalytic activity for the degradation of three dyes (methyl blue (MB), Rhodamine B (RhB), and methyl orange (MO)) [32].

Our research utilized a Cu&POM based complex $[Cu_4(phen)_4(HPO_4)_2(H_2O)_2(OH)_2]\cdot[HPMo_{12}O_{40}]\cdot H_2O$ (abb. Cu-PMo_{12}) (CCDC: 666620) as a bifunctional photocatalyst for the oxidation of toluene and the photodegradation of metronidazole. The use of Cu-PMo_{12} for toluene oxidation achieved high yields and selectivity (100%) for benzaldehyde under conditions of low energy consumption—An unprecedented result with exceptional stability maintained during the cycle test. Moreover, Cu-PMo_{12} was applied to the photodegradation of metronidazole, exhibiting a degradation rate of 0.178. These results indicate that the Cu&POM based complex could be effectively applied as a photocatalyst for organic reactions.

2 Materials and methods

2.1 Materials and physical measurements

All reagents were obtained commercially and utilized as received. Elemental analyses (C, H, and N) were carried out using a Perkin-Elmer 2400 CHN Elemental Analyzer. Gas chromatography (GC) analyses were conducted on a SHIMADZU Gas Chromatograph (GC-2014C) equipped with an auto injector (AOC-20i). UV–visible (UV–Vis) measurements were performed using a TU-1901 Double-beam UV–visible spectrophotometer. The light source for metronidazole degradation was an LED power supply at 400 nm (model: XC-36W900-HTP), while the oxidation of toluene was facilitated by a multichannel photocatalytic reactor (10 W, model: PCX-50C Discover).

2.2 Photocatalytic oxidation of toluene

In a typical experimental setup, 3 mL of toluene and 7 mL of acetonitrile were combined with varying amounts of Cu-PMo_{12} (10, 15, and 20 mg) in a 20 mL photocatalytic vial. The mixture was sparged with oxygen for 10 min to maintain an atmosphere of 1 atm of O_2 under sealed conditions. The reaction was stirred at room temperature and subjected to irradiation with light of specific wavelengths (365, 420, or 450 nm) for durations ranging from 3 to 24 h. Subsequently, the reaction solution was analyzed by gas chromatography to determine the conversion of toluene and the selectivity for benzaldehyde.

For stability tests, the catalyst was precipitated, washed with water and ethanol, and dried at room temperature. This procedure was repeated six times, with each cycle lasting 6 h.

2.3 Photodegradation of metronidazole

The test concentration for metronidazole was set at 100 mg/L. The solution of metronidazole was combined with 10 mL of Cu-PMo_{12} (10 mg) and sonicated for 5 min to ensure uniformity. The mixture then underwent an adsorption–desorption equilibration for 50 min in a dark environment. Following this, degradation was initiated using a 400 nm visible light lamp. Throughout the degradation process, samples were periodically withdrawn and replaced with an equivalent volume of water to maintain consistent dilution. After centrifugal separation, the samples were analyzed using UV–Vis diffuse reflectance spectroscopy (DRS) in the 200–600 nm range. The degradation efficiency was quantified by C/C_0 (C represents the concentration at a specific time, while C_0 denotes the initial concentration).

3 Results and discussion

3.1 Structure and morphological characterization

To elucidate the structure of the Cu&POM based complex, we employed a series of characterization techniques. Initially, the structural representation of Cu-PMo_{12} is depicted in Fig. 1(a), highlighting the assembly of Cu^{2+}, 1,10-phenanthroline, and PMo_{12} units. Fourier transform infrared spectrum of Cu-PMo_{12}, performed using a KBr pellet, revealed the spectral range from 500 to 4,000 cm^{-1} for Cu-PMo_{12}. As illustrated in Fig. 1(b), the PMo_{12} unit displayed four characteristic peaks: 1,058 cm^{-1} for P–O_a (central PO_4 tetrahedron oxygen atoms), 970 cm^{-1} for Mo=O_d (terminal oxygen atoms), 876 cm^{-1} for Mo–Ob–Mo (corner-shared oxygen atoms), and 813 cm^{-1} for Mo–O_c–Mo (edge shared oxygen atoms) [15, 33]. Additional peaks between 1,000 and 1,748 cm^{-1} correspond to vibrations of the aromatic ring in 1,10-phenanthroline [34], and a peak at 3,172 cm^{-1} is attributed to C–H vibrations in 1,10-phenanthroline [35]. Notably, the infrared spectra of Cu-PMo_{12} remained consistent postreaction, affirming the photocatalyst's remarkable stability (Fig. S1 in the Electronic Supplementary Material (ESM)).

High-resolution optical microscopy allowed for the examination of Cu-PMo_{12}'s microcrystal Cu-PMo morphology, revealing uniformly sized microcrystals (approx. 100 μm), as shown in Fig. 1(c). Energy-dispersive spectroscopy (EDS) of Cu-PMo_{12} confirmed the presence of Cu, P, and Mo, further substantiating the successful synthesis of the Cu&POM based complex Cu-PMo_{12} (Fig. 1(d)).

Thermogravimetric analysis (TGA) of Cu-PMo_{12} indicated two distinct phases of weight loss (Fig. S3 in the ESM). The initial phase occurred between room temperature and 200 °C, attributed to the release of coordinated and free water molecules. A significant reduction in mass was observed between 400 and 800 °C, corresponding to the decomposition of phosphomolybdic acid and organic ligands [36].

Moreover, the oxidation states of the elements Cu-PMo_{12} within Cu-PMo_{12} were characterized using X-ray photoelectron spectroscopy (XPS). The spectra Cu-PMo_{12} revealed Cu (2p), Mo (3d), P (2p), C (1s), N (1s), and O (1s) compositions (Fig. 2 and Fig. S2 in the ESM). Specifically, the Cu 2p spectrum (Fig. 2(a)) featured the main Cu $2p_{3/2}$ peak and its satellite at 934.7 and 942.9 eV, respectively, and the main Cu $2p_{1/2}$ peak with its satellite at 954.3 and 962.3 eV. Additionally, two signals at 232.6 and 235.7 eV for Mo^{6+} (Fig. 2(b)), representative of Mo $3d_{3/2}$ and Mo $3d_{5/2}$, were observed [37]. The P 2p XPS spectrum of Cu-PMo_{12} (Fig. 2(c)) showed a binding energy of 133.7 eV, indicative of P–O bonds. The C 1s spectrum was deconvoluted into two peaks, representing C=C at a binding energy of 284.5 eV [38] and C–N at 285.3 eV [39]. Collectively, the XPS data of Cu-PMo_{12} not only confirm the structure of Cu-PMo_{12} but also demonstrate the high oxidation states of Cu and Mo, essential for the oxidation–reduction reactions involved.

The Cu&POM based complex, as a type of Cu-based complex, exhibits photocatalytic activity toward oxidation and photodegradation. The solid state UV–vis DRS spectrum of Cu-PMo_{12}, displayed in Fig. 3(a), shows two distinct absorption peaks. The peak at 306 nm primarily results from the charge transfer transition $\pi\rightarrow\pi^*$ within the fundamental structure of phenanthroline [34]. A plot of $(\alpha h\nu)_{1/2}$ versus $h\nu$ was used to determine the band gap of Cu-PMo_{12}, which was found to be

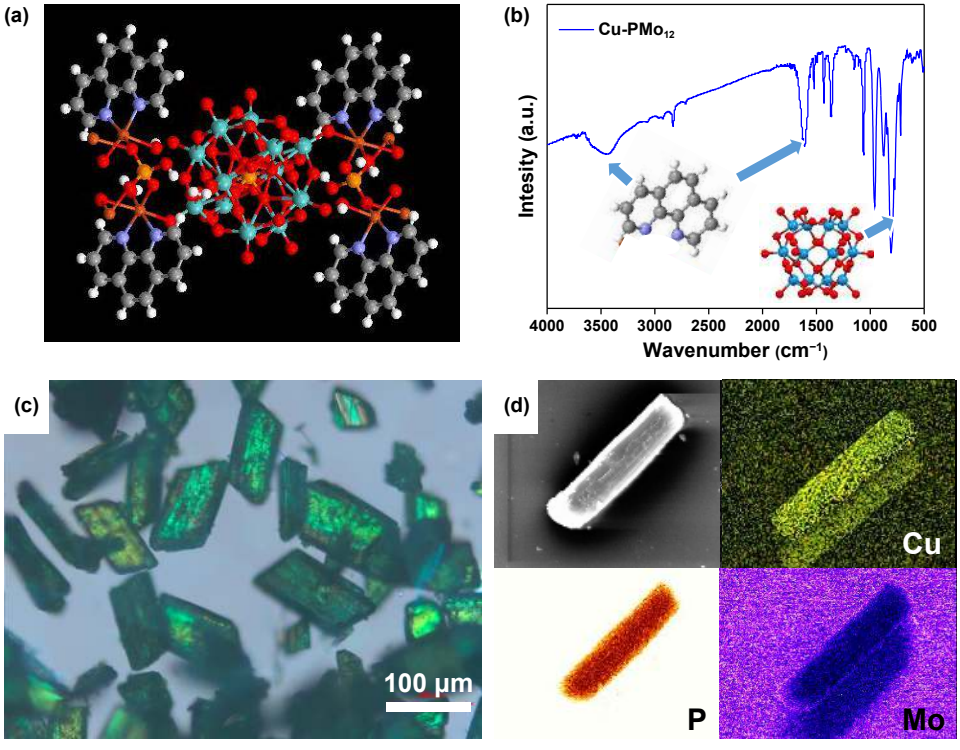

Figure 1 (a) The structure, (b) IR spectrum, (c) high-resolution optical microscope image and (d) the corresponding EDS mapping of of Cu-PMo_{12}.

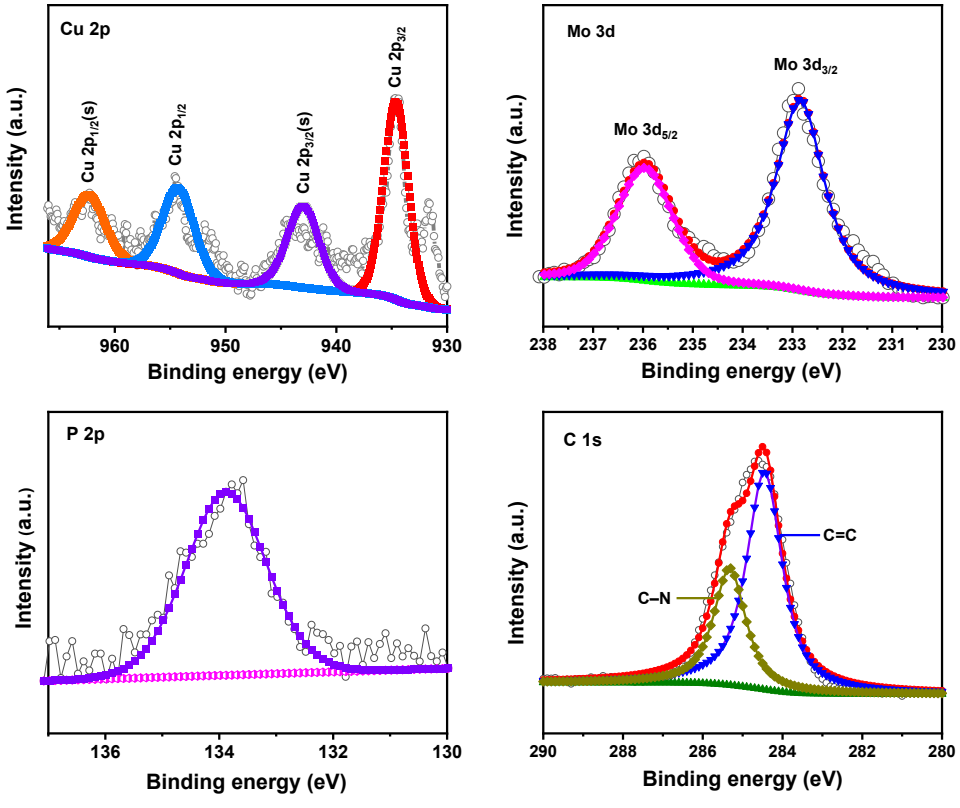

Figure 2 (a) Cu 2p, (b) Mo 3d, (c) P 2p, and (d) C 1s of high-resolution XPS spectra of Cu-PMo_{12}.

2.49 eV (E_g = 2.49 eV), indicating that Cu-PMo_{12} possesses a suitable band gap for semiconductor applications [40]. Furthermore, Mott–Schottky plot with positive slopes confirm that the synthesized material is a typical n-type semiconductor (Fig. 3(b)). The flat band potential of Cu-PMo_{12} relative to the Ag/AgCl electrode is −0.56 V, equating to −0.36 V versus the normal hydrogen electrode (NHE) [41]. Thus, the valence band (EVB) of Cu-PMo_{12} is calculated at 2.13 V ($E_{VB} = E_g + E_{CB}$) [42].

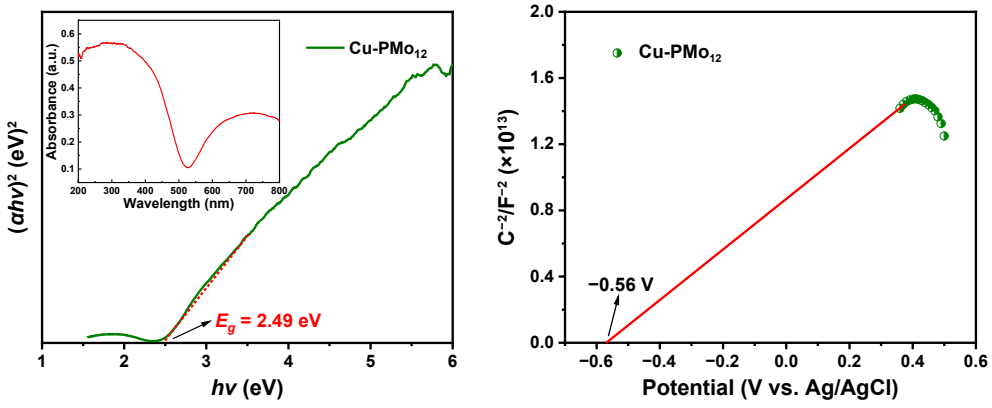

Figure 3 (a) The solid-state UV–vis DRS spectrum and (b) the Mott–Schottky plot of Cu-PMo_{12}.

The E_{VB} and E_g values Cu-PMo_{12} demonstrate that Cu-PMo_{12} is well-suited for photocatalytic applications.

3.2 Photocatalytic oxidation of toluene

Efficient production of the desired product during the photocatalytic oxidation of toluene presents numerous challenges. Inspired by the photocatalytic activity of Cu-PMo_{12}, we oxidized toluene under an oxygen atmosphere, at ambient temperature, and with radiation from a xenon lamp. A series of experiments determined the optimal conditions for this reaction, as detailed in Table 1. The best catalytic effect was observed using 10 mg of Cu-PMo_{12} under a 365 nm light source. Optimal control of the reaction time to 4 h achieved 100% selectivity for benzaldehyde, representing a significant improvement over previous studies [29, 43, 44] (Fig. 4(b)). Notably, no benzoic acid formation was observed when the reaction time was less than 8 h, allowing selective production of benzaldehyde. The selectivity for benzaldehyde reached 15.91 mmol/g at 10 h, superior to the 2.83 mmol/g at 8 h. This increase is attributed to the onset of benzoic acid formation after 8 h. The conversion of toluene gradually increased with the reaction time, reaching 58.7 mmol/g at 24 h, surpassing previous results for photocatalytic toluene oxidation (Fig. 4(c)).

Additionally, Cu-PMo_{12} was utilized to oxidize substituted C–H bonds on other aromatic rings [45]. The conversions of *p*-nitrotoluene, *p*-bromotoluene, *p*-xylene, and homo-trimethylbenzene at 6 h were 10.64, 164.0, 9.1, and 28.56 mmol/g, respectively. Oxidation of alkyl side chains and hydrocarbon double bonds (C=H) on the benzene ring was also effective; for instance, the oxidation of p-bromoethylbenzene and styrene reached conversions of 361 and 30.66 mmol/g, respectively (Table S1 in the ESM).

Cycle testing was conducted to further evaluate the durability of Cu-PMo_{12}. After a 6 h reaction, the catalysts underwent five additional cycles of testing and recycling, using centrifugation. Throughout these cycles, there was no significant decrease in either the conversion rate or the selectivity toward benzaldehyde (Fig. 4(d)).

3.3 Photodegradation of metronidazole

Cu-PMo_{12} was utilized as a catalyst for the photodegradation of the antibiotic metronidazole in aqueous solution under illumination from a 400 nm visible light lamp. Figure S4 in the ESM illustrates the absorbance results of the metronidazole solution under various conditions. After introducing the catalyst to the solution and allowing it to react for 150 min, as shown in Fig. 5, C/C_0 decreased to 0.26. Subsequently, upon the addition of a sodium chloride solution (35.5 mg of NaCl added achieving a concentration of 0.1 mol/L), the C/C_0 value further decreased to 0.178, maintaining the

Table 1 Conversion rate of toluene and selectivity of benzaldehyde under different conditions

Reaction conditions				Total yield (mmol/g)[a]	Benzaldehyde (mmol/g)[a]	Benzaldehyde selectivity
Catalyst type	Catalyst weight (mg)	Light wavelength (nm)	Reation time (h)			
Cu-PMo_{12}	10	365	3	0.92	0.92	100%
$CuSO_4{\cdot}5H_2O$	10	365	3	0.105	0.105	100%
$H_3PO_4{\cdot}12MoO_3$	10	365	3	7.83	6.6	84.30%
Cu-PMo_{12}	10	365	10	22.89	15.91	69.50%
Cu-PMo_{12}[b]	10	365	10	16.4	5.99	36.50%
Cu-PMo_{12}	10	365	4	1.21	1.21	100%
Cu-PMo_{12}	10	420	4	1.03	1.03	100%
Cu-PMo_{12}	10	450	4	0.85	0.85	100%
Cu-PMo_{12}	10	365	4	1.21	1.21	100%
Cu-PMo_{12}	15	365	4	1.95	1.505	77.20%
Cu-PMo_{12}	20	365	4	2.76	2.41	87.30%

[a]The yield was obtained by GC; [b]without any solvent, the substrate was applied as the solvent.

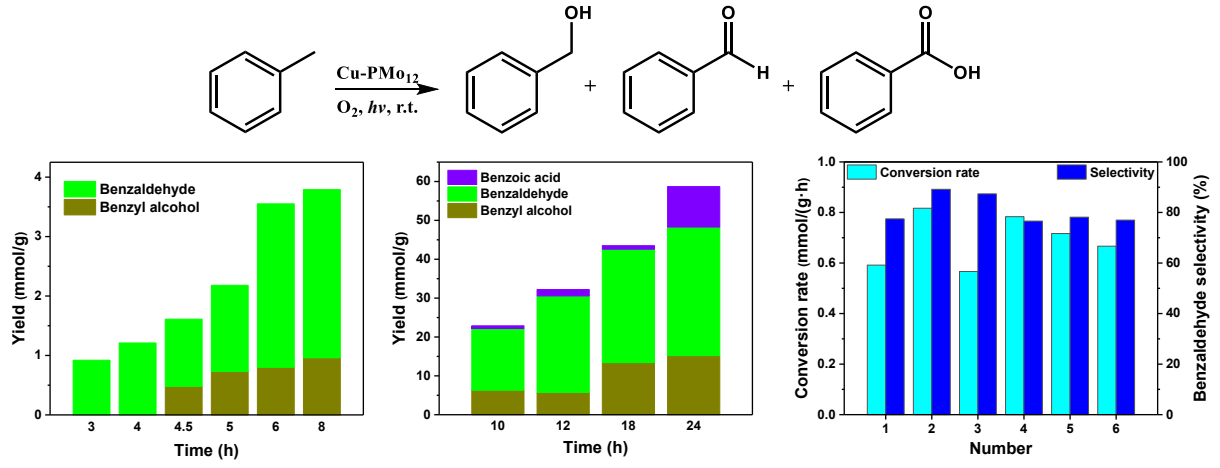

Figure 4 (a) Photocatalytic oxidation of toluene. Conversion rate of different products of toluene: (b) from 3 to 8 h; (c) from 10 to 24 h. (d) The catalytic durability of Cu-PMo_{12}.

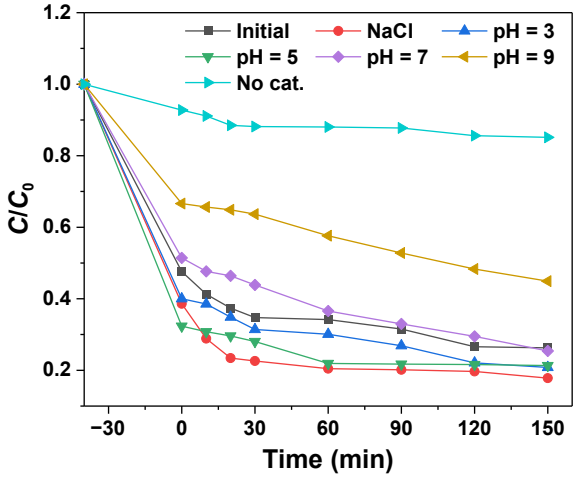

Figure 5 Effect of the catalyst on the degradation of metronidazole under different conditions under visible light.

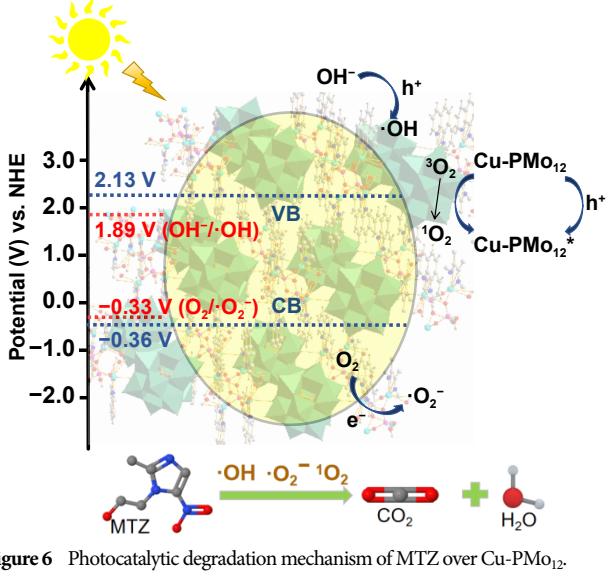

Figure 6 Photocatalytic degradation mechanism of MTZ over Cu-PMo_{12}.

initial metronidazole concentration at 100 mg/L. This data demonstrates that the photodegradation of metronidazole under visible light is enhanced by the addition of NaCl, likely due to an increase in the ionic strength from chloride ions, which accelerates the catalytic decomposition of metronidazole [46]. The negligible degradation observed without Cu-PMo_{12} underscores the indispensability of the catalyst.

Further experimentation revealed that varying the pH of the solution containing metronidazole influenced the degradation outcomes significantly. As the reaction time neared 150 min, C/C_0 values of 0.2, 0.22, 0.25, and 0.45 were recorded at pH levels of 3, 5, 7, and 9, respectively. These results indicate that acidic conditions are more conducive to the degradation of metronidazole in aqueous solutions, as evidenced by substantially lower C/C_0 values compared to neutral and alkaline conditions. Changes in pH likely affect the electrochemical properties of both metronidazole and the catalyst, which could explain the observed differences. The electrostatic interactions between the complex and metronidazole, resulting from the liberation of charge in the solution, contribute to the variability in degradation efficacy across different pH values [47].

Based on the research findings, we propose the possible degradation mechanisms of Cu-PMo_{12}, as illustrated in Fig. 6. POM based compounds and semiconductor materials exhibit similar photocatalytic properties [48, 49]. Notably, the valence and conduction bands of semiconductors correlate with the highest occupied molecular orbital (HOMO) and lowest unoccupied molecular orbital (LUMO) energy levels in POM compounds [50, 51]. Initially, metronidazole is absorbed onto the surface of Cu-PMo_{12} in the dark, facilitated by the appropriate band gap (E_g = 2.49 eV). Under visible light, electrons may transfer from O^{2-} to Mo^{6+} via Mo–O–Mo bonds, generating a highly oxidized excited state. This state efficiently transfers energy to molecular oxygen (O_2), forming singlet oxygen ($^1O_2$). The process also produces a hole–electron pair (hole at $O^-$and electron at Mo_5^+), similar to those in semiconducting metal oxides. The conduction band potential of Cu-PMo_{12} (E_{CB} = −0.36 V) is lower than the potential of $O_2/\cdot O^{2-}$ (−0.33 V vs. NHE), facilitating the production of superoxide radicals ($\cdot O^{2-}$) through the reduction of dissolved O_2 by photogenerated electrons [52, 53]. Additionally, the valence band potential of Cu-PMo_{12} (E_{VB} = 2.13 V) exceeds that of $OH^-/\cdot OH$ (1.89 V vs. NHE), enabling the photogenerated holes to oxidize hydroxide ions (OH^-) on the material's surface to hydroxyl radicals (·OH). These reactive oxygen species further decompose metronidazole into low-toxicity intermediates, and ultimately into

carbon dioxide and water. The specific intermediate products have not yet been identified, necessitating further investigation to elucidate the exact photocatalytic mechanism.

4 Conclusions

In summary, we have synthesized a Cu&POM based complex incorporating PMo_{12} and 1,10-phenanthroline. This complex exhibits outstanding photocatalytic performance, particularly in toluene oxidation tests where it achieved 100% selectivity for benzaldehyde within 4 h, without producing benzoic acid for up to 8 h. After 24 h, it reached a conversion rate of 58.7 mmol/g, an unprecedented result that was consistently maintained even after six cycles. The complex also proved effective in catalyzing the photodegradation of metronidazole, achieving a degradation rate of 0.178 with minimal energy consumption. These achievements highlight the potential of Cu&POM based complexes in enhancing photocatalytic properties for applications in chemical engineering and water treatment. Future studies could expand on this research by exploring the oxidation of additional aromatic hydrocarbons and the degradation of other antibiotics, thereby broadening the applicability of such complexes in environmental management and sustainable chemical processes.

Electronic Supplementary Material: Supplementary material (synthesis method, FT-IR, XPS spectra, TGA curves and so on) is available in the online version of this article at https://doi.org/10.26599/POM.2024.9140067.

Data availability

All data needed to support the conclusions in the paper are presented in the manuscript and/or the Electronic Supplementary Material. Additional data related to this paper may be requested from the corresponding author upon request.

Acknowledgements

This study was supported by the National Natural Science Foundation of China (Nos. 22171024 and 21801014). The Analysis and Testing Center of Beijing Institute of Technology is highly appreciated for their instrument support.

Declaration of competing interest

The authors declare that they have no known competing financial interests or personal relationships that could have appeared to influence the work reported in this paper.

Author contribution statement

Fei Wang, Jiejie Ping, and Danyang He were responsible for designing the research methodology, analyzing the data, and conducting in-depth investigations. Wenhui Shang focused on writing the paper, while Chaojun Jing, Nan Wang, Muling Zeng, and Zhiyu Jia provided the necessary resources and supervision to ensure the smooth progress of the research.

References

[1] Patel, M.; Kumar, R.; Kishor, K.; Mlsna, T.; Pittman, C. U. Jr.; Mohan, D. Pharmaceuticals of emerging concern in aquatic systems: Chemistry, occurrence, effects, and removal methods. *Chem. Rev.* **2019**, *119*, 3510–3673.

[2] Rojas, S.; Horcajada, P. Metal-organic frameworks for the removal of emerging organic contaminants in water. *Chem. Rev.* **2020**, *120*, 8378–8415.

[3] Lin, H. F.; Li, L. P.; Zhao, M. L.; Huang, X. S.; Chen, X. M.; Li, G. S.; Yu, R. C. Synthesis of high-quality brookite TiO_2 single-crystalline nanosheets with specific facets exposed: Tuning catalysts from inert to highly reactive. *J. Am. Chem. Soc.* **2012**, *134*, 8328–8331.

[4] Wu, Q. P.; Van De Krol, R. Selective photoreduction of nitric oxide to nitrogen by nanostructured TiO_2 photocatalysts: Role of oxygen vacancies and iron dopant. *J. Am. Chem. Soc.* **2012**, *134*, 9369–9375.

[5] Seidensticker, S.; Zarfl, C.; Cirpka, O. A.; Fellenberg, G.; Grathwohl, P. Shift in mass transfer of wastewater contaminants from microplastics in the presence of dissolved substances. *Environ. Sci. Technol.* **2017**, *51*, 12254–12263.

[6] Malakootian, M.; Kannan, K.; Gharaghani, M. A.; Dehdarirad, A.; Nasiri, A.; Shahamat, Y. D.; Mahdizadeh, H. Removal of metronidazole from wastewater by Fe/charcoal micro electrolysis fluidized bed reactor. *J. Environ. Chem. Eng.* **2019**, *7*, 103457.

[7] Kompa, A.; Mahesha, M. G.; Kekuda, D.; Rao, K. M. Spectroscopic investigation of defects in spin coated titania based thin films for photocatalytic applications. *J. Solid State Chem.* **2021**, *303*, 122488.

[8] Mohsen, M.; Naeem, I.; Awaad, M.; Tantawy, H.; Baraka, A. A cadmium-imidazole coordination polymer as solid state buffering material: Synthesis, characterization and its use for photocatalytic degradation of ionic dyes. *J. Solid State Chem.* **2020**, *289*, 121493.

[9] Wen, X.; Wang, W. Q.; Ye, Q. P.; Zhou, Y. F.; Yang, J.; Sun, N.; Tan, Y. G.; Wang, W. B.; Hou, Y.; Yan, C. J. One-step synthesis of rice husk carbon with dangling CC bonds loaded g-C_3N_4 for enhanced photocatalytic degradation. *J. Clean. Prod.* **2020**, *272*, 122625.

[10] Saidi, I.; Soutrel, I.; Floner, D.; Fourcade, F.; Bellakhal, N.; Amrane, A.; Geneste, F. Indirect electroreduction as pretreatment to enhance biodegradability of metronidazole. *J. Hazard. Mater.* **2014**, *278*, 172–179.

[11] Cao, J. Y.; Li, J. J.; Chu, W.; Cen, W. L. Facile synthesis of Mn-doped BiOCl for metronidazole photodegradation: Optimization, degradation pathway, and mechanism. *Chem. Eng. J.* **2020**, *400*, 125813.

[12] Worathitanon, C.; Jangyubol, K.; Ruengrung, P.; Donphai, W.; Klysubun, W.; Chanlek, N.; Prasitchoke, P.; Chareonpanich, M. High performance visible-light responsive Chl-Cu/ZnO catalysts for photodegradation of rhodamine B. *Appl. Catal. B: Environ.* **2019**, *241*, 359–366.

[13] Liu, W. F.; Qiu, Q. M.; Zhang, M.; Su, Z. M.; An, Q. Q.; Lv, H. J.; Jia, Z. Y.; Yang, G. Y. Two new Cu-based borate catalysts with cubic supramolecular cages for efficient catalytic hydrogen evolution. *Dalton Trans.* **2020**, *49*, 10156–10161.

[14] Lu, F. D.; Liu, D.; Zhu, L.; Lu, L. Q.; Yang, Q.; Zhou, Q. Q.; Wei, Y.; Lan, Y.; Xiao, W. J. Asymmetric propargylic radical cyanation enabled by dual organophotoredox and copper catalysis. *J. Am. Chem. Soc.* **2019**, *141*, 6167–6172.

[15] Li, P. H.; Wang, Y. Y.; Wang, X.; Wang, Y.; Liu, Y.; Huang, K. K.; Hu, J.; Duan, L. M.; Hu, C. W.; Liu, J. H. Selective oxidation of benzylic C-H bonds catalyzed by Cu(II)/{PMo_{12}}. *J. Org. Chem.* **2020**, *85*, 3101–3109.

[16] Li, S. J.; Li, N.; Li, G.; Ma, Y. B.; Huang, M. Y.; Xia, Q. C.; Zhao, Q. Y.; Chen, X. N. Silver-modified polyniobotungstate for the visible light-induced simultaneous cleavage of C-C and C-N bonds. *Polyoxometalates* **2023**, *2*, 9140024.

[17] Zhang, G. Y.; Wang, Y. F. Metal-oxide clusters with semiconductive heterojunction counterparts. *Polyoxometalates* **2023**, *2*, 9140020.

[18] Ma, Y. B.; Gao, F.; Xiao, W. R.; Li, N.; Li, S. J.; Yu, B.; Chen, X. N. Two transition-metal-modified Nb/W mixed-addendum polyoxometalates for visible-light-mediated aerobic benzylic C-H

oxidations. *Chin. Chem. Lett.* **2022**, *33*, 4395–4399.
[19] Chang, Q.; Meng, X. Y.; Ruan, W. J.; Feng, Y. Q.; Li, R.; Zhu, J. Y.; Ding, Y.; Lv, H. J.; Wang, W.; Chen, G. Y. et al. Metal-organic cages with $\{SiW_9Ni_4\}$ polyoxotungstate nodes. *Angew. Chem., Int. Ed.* **2022**, *61*, e202117637.
[20] Hu, Q. Y.; Chen, S. S.; Wågberg, T.; Zhou, H. S.; Li, S. J.; Li, Y. D.; Tan, Y. L.; Hu, W. Q.; Ding, Y.; Han, X. B. Developing insoluble polyoxometalate clusters to bridge homogeneous and heterogeneous water oxidation photocatalysis. *Angew. Chem., Int. Ed.* **2023**, *62*, e202303290.
[21] Lai, S. Y.; Ng, K. H.; Cheng, C. K.; Nur, H.; Nurhadi, M.; Arumugam, M. Photocatalytic remediation of organic waste over Keggin-based polyoxometalate materials: A review. *Chemosphere* **2021**, *263*, 128244.
[22] Ma, P. T.; Hu, F.; Wang, J. P.; Niu, J. Y. Carboxylate covalently modified polyoxometalates: From synthesis, structural diversity to applications. *Coord. Chem. Rev.* **2019**, *378*, 281–309.
[23] Shi, Z. L.; Li, J.; Han, Q. X.; Shi, X. Y.; Si, C.; Niu, G. Q.; Ma, P. T.; Li, M. X. Polyoxometalate-supported aminocatalyst for the photocatalytic direct synthesis of imines from alkenes and amines. *Inorg. Chem.* **2019**, *58*, 12529–12533.
[24] Wang, Y. J.; Zhuang, G. L.; Zhang, J. W.; Luo, F.; Cheng, X.; Sun, F. L.; Fu, S. S.; Lu, T. B.; Zhang, Z. M. Co-dissolved isostructural polyoxovanadates to construct single-atom-site catalysts for efficient CO_2 photoreduction. *Angew. Chem., Int. Ed.* **2023**, *62*, e202216592.
[25] Lan, Q.; Jin, S. J.; Yang, B. H.; Zhao, Q.; Si, C. L.; Xie, H. Q.; Zhang, Z. M. Metal-Oxo cluster catalysts for photocatalytic water splitting and carbon dioxide reduction. *Trans. Tianjin Univ.* **2022**, *28*, 214–225.
[26] Han, X. B.; Zhang, Z. M.; Zhang, T.; Li, Y. G.; Lin, W. B.; You, W. S.; Su, Z. M.; Wang, E. B. Polyoxometalate-based cobalt-phosphate molecular catalysts for visible light-driven water oxidation. *J. Am. Chem. Soc.* **2014**, *136*, 5359–5366.
[27] Li, Q.; Wei, Y. G.; Hao, J.; Zhu, Y. L.; Wang, L. S. Unexpected C=C bond formation via doubly dehydrogenative coupling of two saturated sp^3 C-H bonds activated with a polymolybdate. *J. Am. Chem. Soc.* **2007**, *129*, 5810–5811.
[28] Li, J.; He, J. C.; Si, C.; Li, M. X.; Han, Q. X.; Wang, Z. L.; Zhao, J. W. Special-selective C–H oxidation of toluene to benzaldehyde by a hybrid polyoxometalate photocatalyst including a rare $[P_6W_{48}Fe_6O_{180}]^{30-}$ anion. *J. Catal.* **2020**, *392*, 244–253.
[29] Yu, B.; Zhang, S. M.; Wang, X. Helical Microporous nanorods assembled by polyoxometalate clusters for the photocatalytic oxidation of toluene. *Angew. Chem., Int. Ed.* **2021**, *60*, 17404–17409.
[30] Wang, J.; Chen, Y.; Cheng, N.; Feng, L.; Gu, B. H.; Liu, Y. Multivalent supramolecular self-assembly between β-cyclodextrin derivatives and polyoxometalate for photodegradation of dyes and antibiotics. *ACS Appl. Bio Mater.* **2019**, *2*, 5898–5904.
[31] Pal, D.; Biswas, S.; Nayak, A. K.; Pal, A. Application of polyoxometalates and their composites for the degradation of antibiotics in water medium. *Water. Emerg. Contam. Nanoplast.* **2023**, *2*, 21.
[32] Gong, L. G.; Liu, J. M.; Yu, K.; Su, Z. H.; Zhou, B. B. Two new $\{As_3W_3\}$ polyoxometalates decorated with metal-phen complexes: Synthesis, structure and properties. *J. Solid State Chem.* **2019**, *270*, 280–286.
[33] Wu, Y. Y.; Dong, J.; Liu, C. P.; Jing, X. T.; Liu, H. F.; Guo, Y.; Chi, Y. N.; Hu, C. W. Reduced polyoxomolybdate immobilized on reduced graphene oxide for rapid catalytic decontamination of a sulfur mustard simulant. *Dalton Trans.* **2021**, *50*, 9796–9803.
[34] Wang, Q. Q.; Wang, D. X.; Wu, Y. L.; Li, L. X.; Sun, X. Y. Synthesis of polyoxometalate-based complexes and photocatalytic degradation of metronidazole. *J. Solid State Chem.* **2022**, *309*, 122966.
[35] Wu, L. Z.; Ma, H. Y.; Han, Z. G.; Li, C. X. Synthesis, structure and property of a new inorganic-organic hybrid compound $[Cu(phen)_2][Cu(phen)H_2O]_2[Mo_5P_2O_{23}]\cdot 3.5H_2O$. *Solid State Sci.* **2009**, *11*, 43–48.
[36] Bajpe, S. R.; Henke, S.; Lee, J. H.; Bristowe, P. D.; Cheetham, A. K. Disorder and polymorphism in Cu(II)-polyoxometalate complexes: $[Cu_{1.5}(H_2O)_{7.5}PW_{12}O_{40}]\cdot 4.75H_2O$, *cis*- & *trans*-$[Cu_2(H_2O)_{10}SiW_{12}O_{40}]\cdot 6H_2O$. *CrystEngComm* **2016**, *18*, 5327–5332.
[37] Shi, S. Y.; Chen, L. Y.; Zhu, T. H.; Cui, X. B. Two compounds constructed from Strandberg-type polyoxoanions, metals and organic ligands. *J. Coord. Chem.* **2017**, *70*, 3823–3836.
[38] Han, Z. Y.; Li, X. Y.; Li, Q.; Li, H. S.; Xu, J.; Li, N.; Zhao, G. X.; Wang, X.; Li, H. L.; Li, S. D. Construction of the POMOF@polypyrrole composite with enhanced ion diffusion and capacitive contribution for high-performance lithium-ion batteries. *ACS Appl. Mater. Interfaces* **2021**, *13*, 6265–6275.
[39] Wei, X. Y.; Wei, J. W.; Huang, L. P.; Yan, T. T.; Luo, F. Facile fabricating the polyoxometalates functionalized graphene nanocomposite applied in electrocatalytic reduction. *Inorg. Chem. Commun.* **2017**, *81*, 10–14.
[40] Yan, L. J.; Wang, Q.; Qu, W. Q.; Yan, T. T.; Li, H. R.; Wang, P. L.; Zhang, D. S. Tuning $Ti^{\delta+}$-Vo··-$Pt^{\delta+}$ interfaces over Pt/TiO_2 catalysts for efficient photocatalytic oxidation of toluene. *Chem. Eng. J.* **2022**, *431*, 134209.
[41] Xu, C. Y.; Pan, Y. T.; Wan, G.; Liu, H.; Wang, L.; Zhou, H.; Yu, S. H.; Jiang, H. L. Turning on visible-light photocatalytic C−H oxidation over metal-organic frameworks by introducing metal-to-cluster charge transfer. *J. Am. Chem. Soc.* **2019**, *141*, 19110–19117.
[42] Shao, Q.; Lin, H. P.; Shao, M. W. Determining locations of conduction bands and valence bands of semiconductor nanoparticles based on their band gaps. *ACS Omega* **2020**, *5*, 10297–10300.
[43] Kaeding, W. W.; Lindblom, R. O.; Temple, R. G.; Mahon, H. I. Oxidation of toluene and other alkylated aromatic hydrocarbons to benzoic acids and phenols. *Ind. Eng. Chem. Process Des. Dev.* **1965**, *4*, 97–101.
[44] Cao, X.; Chen, Z.; Lin, R.; Cheong, W. C.; Liu, S. J.; Zhang, J.; Peng, Q.; Chen, C.; Han, T.; Tong, X. J. et al. A photochromic composite with enhanced carrier separation for the photocatalytic activation of benzylic C-H bonds in toluene. *Nat. Catal.* **2018**, *1*, 704–710.
[45] Xiao, W. R.; Li, S. J.; Zhao, Y.; Ma, Y. B.; Li, N.; Zhang, J.; Chen, X. N. Multinuclear transition metal-containing polyoxometalates constructed from Nb/W mixed-addendum precursors: Synthesis, structures and catalytic performance. *Dalton Trans.* **2021**, *50*, 8690–8695.
[46] Mousavi, S. A.; Janjani, H. Antibiotics adsorption from aqueous solutions using carbon nanotubes: A systematic review. *Toxin Rev.* **2020**, *39*, 87–98.
[47] Xu, L. J.; Yang, Y. J.; Li, W. Y.; Tao, Y. J.; Sui, Z. G.; Song, S.; Yang, J. Three-dimensional macroporous graphene-wrapped zero-valent copper nanoparticles as efficient micro-electrolysis-promoted Fenton-like catalysts for metronidazole removal. *Sci. Total Environ.* **2019**, *658*, 219–233.
[48] Meziani, D.; Abdmeziem, K.; Bouacida, S.; Trari, M. Photo-electrochemical and physical characterizations of a new single crystal POM-based material. *Application in photocatalysis. J. Mol. Struct.* **2016**, *1125*, 540–545.
[49] Gurrentz, J. M.; Rose, M. J. Covalent attachment of polyoxometalates to passivated Si(111) substrates: A stable and electronic defect-free Si|POM platform. *J. Phys. Chem. C* **2021**, *125*, 14287–14298.
[50] Zhang, J.; Zhan, M. Y.; Zheng, L. L.; Zhang, C.; Liu, G. D.; Sha, J. Q.; Liu, S. J.; Tian, S. FeOCl/POM heterojunctions with excellent Fenton catalytic performance via different mechanisms. *Inorg. Chem.* **2019**, *58*, 250–258.
[51] Liu, J. L.; Shi, W. X.; Wang, X. ZnO-POM cluster sub-1 nm nanosheets as robust catalysts for the oxidation of thioethers at room temperature. *J. Am. Chem. Soc.* **2021**, *143*, 16217–16225.
[52] Gupta, R.; Kumar, G.; Gupta, R. Encapsulation-led adsorption of

neutral dyes and complete photodegradation of cationic dyes and antipsychotic drugs by lanthanide-based macrocycles. *Inorg. Chem.* **2022**, *61*, 7682–7699.

[53] Zhang, X. W.; Wang, F.; Wang, C. C.; Wang, P.; Fu, H. F.; Zhao, C. Photocatalysis activation of peroxodisulfate over the supported Fe_3O_4 catalyst derived from MIL-88A(Fe) for efficient tetracycline hydrochloride degradation. *Chem. Eng. J.* **2021**, *426*, 131927.

Fei Wang is a Master's student at the School of Chemistry and Chemical Engineering, Beijing Institute of Technology. Her research interests are centered around the applied study of polyoxometalate composites and their role in catalytic chemistry.

Zhiyu Jia is an associate professor at the school of chemistry and chemical Engineering, Beijing Institute of Technology. His research is focused on the synthesis of polyoxometalates-based functional materials and their applications in the field of electrocatalysis and photocatalysis.